LAWRENCE
LIVERMORE
NATIONAL
LABORATORY

UCRL-CONF-216946

Radiation-driven hydrodynamics of long pulse hohlraums on the National Ignition Facility

D. L. Dewald, O. L. Landen, L. J. Suter, J. Schein, J. Holder, K. Campbell, S. H. Glenzer, J. W. McDonald, C. Niemann, A. J. Mackinnon, M. S. Schneider, C. Haynam, D. Hinkel, B. A. Hammel

November 9, 2005

47th Annual Meeting of the Division of Plasma Physics
Denver, CO, United States
October 24, 2005 through October 28, 2005

Disclaimer

This document was prepared as an account of work sponsored by an agency of the United States Government. Neither the United States Government nor the University of California nor any of their employees, makes any warranty, express or implied, or assumes any legal liability or responsibility for the accuracy, completeness, or usefulness of any information, apparatus, product, or process disclosed, or represents that its use would not infringe privately owned rights. Reference herein to any specific commercial product, process, or service by trade name, trademark, manufacturer, or otherwise, does not necessarily constitute or imply its endorsement, recommendation, or favoring by the United States Government or the University of California. The views and opinions of authors expressed herein do not necessarily state or reflect those of the United States Government or the University of California, and shall not be used for advertising or product endorsement purposes.

Radiation-driven hydrodynamics of long pulse hohlraums on the National Ignition Facility

E.L. Dewald, O.L. Landen, L.J. Suter, J. Schein, J. Holder, K. Campbell, S.H. Glenzer, J.W. McDonald, C. Niemann, A.J. Mackinnon, M.S. Schneider, C. Haynam, D. Hinkel, and B.A. Hammel

LLNL, P.O. Box 808, Livermore, CA 94550

Abstract

The first hohlraum experiments on the National Ignition Facility (NIF) using the first four laser beams have activated the indirect drive experimental capabilities and tested radiation temperature limits imposed by hohlraum plasma filling. Vacuum hohlraums have been irradiated with laser powers up to 6 TW, 1 ns to 9 ns long square pulses and energies of up to 17 kJ to activate several diagnostics, to study the hohlraum radiation temperature scaling with the laser power and hohlraum size, and to make contact with hohlraum experiments performed at the NOVA and Omega laser facilities. Furthermore, for a variety of hohlraum sizes and pulse lengths, the measured x-ray flux shows signatures of plasma filling that coincide with hard x-ray emission from plasma streaming out of the hohlraum. These observations agree with hydrodynamic simulations and with analytical modeling that includes hydrodynamic and coronal radiative losses. The modeling predicts radiation temperature limits on full NIF (1.8 MJ) that are significantly greater than required for ignition hohlraums.

PACS numbers: 52.50.Jm, 52.40.Nk, 52.58.Ns, 52.70.Kz

1. Introduction

The soft x-ray environment created in high-Z hohlraums heated by energetic laser beams, that enter the hohlraums through their Laser Entrance Holes (LEH), is used to drive fuel capsules in indirect-drive inertial confinement fusion (ICF) experiments and to drive physics packages in high energy density (HED) studies. In present indirect drive Inertial Confinement Fusion (ICF) designs the fuel capsule is placed inside the hohlraum [1]. The hohlraum converts the drive laser beams into soft x rays that are used to compress a deuterium-tritium filled (DT) capsule and drive it to ignition and burn. For ignition experiments the high-Z hohlraums contain a mid-to-low Z fill to slow down the hohlraum wall plasma that may otherwise compromise capsule compression symmetry and consequently its ignition [1,2]. The physics of hohlraum energetics studies the laser propagation and absorption in the hohlraum, the conversion efficiency from laser energy into soft x rays and the radiation losses to the hohlraum walls and out of the laser entrance holes (LEH) [3]. Many HED applications [4,5] require a long sustained soft x-ray drive [6,7]. In conditions of efficient heating of the HED package the internal hohlraum radiation flux may begin to drop or roll-over, even before the laser pulse terminates. This occurs when the ablated hohlraum wall plasma reaches a density threshold that prevents the laser from propagating into the hohlraum due to absorption or backscattering. It was originally proposed [8] that this roll-over time τ is determined by laser-plasma instabilities when the plasma density approaches 0.1 n_c, where n_c [cm^{-3}]= 1.1 10^{21} /λ^2[μm^2] is the critical density for laser light of wavelength λ. However, hohlraum experiments with short laser pulse duration have performed properly well beyond the time at which they fill to 0.1 n_c [9,10] indicating that a critical experimental

test of hohlraum fill [11,12] modeling is required for assessing long radiation drive options for HED. Current simulations indicate that hohlraums used in ICF are optimized to drive a fusion capsule to ignition before reaching the x-ray production limits [2].

The National Ignition Facility (NIF) that is currently under construction [13] is a 192 laser beam system that is designed to deliver up to 1.8 MJ of energy at a wavelength of λ_0 = 351 nm. The laser is designed to first achieve indirect drive ICF and will also be used for a variety of High Energy Density (HED) experiments [6]. After the first available four NIF laser beams that form quad 31B were successfully activated, the first hohlraum energetics related experiments Laser-Plasma Interaction (LPI) were performed successfully [14]. In this paper we will present the first hohlraum experiments recently performed on NIF.

The vacuum hohlraum experiments were designed to activate a suite of hohlraum drive diagnostics and to make contact with the hohlraum database obtained at the NOVA and Omega laser facilities [9]. Furthermore, using the unique capability of the NIF laser to deliver long, high energy pulses of up to 20 ns in length, models of extreme hohlraum plasma filling were tested in this study. These models are used to predict hohlraum radiation production limits that are important for designing both future ICF and HED physics experiments.

2. Experiments on NIF

Figure 1 shows the layout used in the first NIF hohlraum experiments. We used cylindrical empty Au hohlraums of various sizes with a single laser entrance hole (LEH).

The hohlraum back wall is irradiated with the four laser beams (λ_0=351 nm) effectively forming an f/8 cone that propagates along the hohlraum axis (see Fig. 1). Full aperture CPP phase plates [15] and polarization smoothing [16] were installed on the laser beams providing a uniform intensity profile spot with a 0.5 mm diameter with best focus placed at the LEH. Constant power (flattop) laser pulses with 100 ps rise and fall times were used with energies between 5 and 17 kJ and pulse lengths between 2 and 9 ns. Several hohlraum sizes were employed between scales 3/4 (1.2 mm diameter, 1.1 mm long) and 3/2 (2.4 mm diameter, 2.3 mm long). All Au hohlraum walls were 5 μm thick, backed by a 100 μm CH coating, allowing us to measure spatially resolved Au L-shell emission (> 9 keV) and to infer the hohlraum plasma fill dynamics [17]. In these experiments the gated framing camera was filtered for photon energies > 6 keV with 100 μm Al, however when viewing side-on through the 5 μm thick hohlraum Au walls the total filtering transmits > 9 keV x rays.

During these first hohlraum experiments on NIF the hohlraum soft and hard x ray drive diagnostics capabilities were activated (Fig. 1). The hohlraum radiation temperature was measured with temporal and spectral resolution through the LEH at 21.6° with an 18-channel absolutely calibrated soft x ray power diagnostic, Dante [18]. Dante has a partial view of the initial laser spots on the hohlraum back wall and provides a measure of the radiation flux that includes both the primary laser-plasma emission and the re-emitting walls (see Fig. 3). The hot electron production inside the hohlraum was inferred from 20-100 keV absolutely calibrated x ray spectra of the electron bremsstrahlung emission [19] spectrally resolved with 8 channels. The laser energy backscattered inside the laser final focusing lenses and outside the lenses within a 20° angle was measured with a Full

Aperture Backscattering Station (FABS) [20] and a Near Backscattering Imager (NBI) [21], respectively. Streak cameras connected to spectrometers in FABS measure time and spectrally resolved stimulated Brillouin and Raman Backscattering Spectra (SBS, SRS). A static x ray imager (SXI) confirmed that the beams propagate through the LEH without striking the outside walls of the hohlraum.

A series of experiments using 2 ns flattop pulses and variable laser energy in the 5-13 kJ range was first performed to measure the radiation temperature scaling with laser power and hohlraum size, ranging between scale 3/4 and scale 1, in a regime similar to previous hohlraum experiments [3,9,10] where minimal plasma filling is expected. Hohlraum plasma filling [11, 12] was studied for longer laser pulses of 6 and 9 ns with up to 17 kJ energy in larger scales 1 to 3/2 hohlraums. The thin wall imaging and Dante measurements were compared to 2-dimensional LASNEX [22] radiation-hydrodynamics simulations to model radiation and plasma hydrodynamics. The simulations are performed using the exact hohlraum geometry, measured laser power history [23], and a radially symmetric approximation to the combined spatial profile of the slightly diverging 4 beams.

3. Results and discussion

3.1 Measured levels of laser backscattering and hot electron fractions

For all vacuum hohlraum experiments performed at intensities up to $3x10^{15}$ W/cm^2 the laser backscattering was negligible for both SRS (< 0.05%) and SBS (< 0.6%). These backscattering values were roughly one order of magnitude smaller than those measured

in hohlraum experiments performed at the Nova laser facilities at similar laser intensities, spatial laser beam smoothing, and hohlraum radiation temperatures [2]. This may be due to Nova and Omega vacuum hohlraums being irradiated by beams incident at 40° vs normal to the hohlraum wall on NIF, leading to shorter effective scale lengths, higher flow gradients, and hence lower laser-plasma instability gain-length products for the NIF-case. Another possible explanation is the application of polarization smoothing on NIF. Future experiments comparing backscattering with and without smoothing may help to better understand these observations.

Figure 2 shows hot electron fraction measurements for the vacuum hohlraum experiments on NIF [24] larger than scale-3/4 as well as results from previous NOVA experiments. Similar to laser backscattering the measured hot electron fraction was <~1% in all hohlraums except the smallest, scale-¾ hohlraum where it was 4%. The measurements show that the hot electron fraction increases with the laser intensity and that is considerably enhanced in the hohlraums that fill with plasma. The measured hot electron temperature was 30 keV. These values are consistent with the previous Nova experiments [2], as well as with the measured SRS in the present experiments. Moreover, at the laser intensities required for the ICF design ($\leq 10^{15}$ W/cm^2) the measured hot electron fraction is within the required levels for similar hot electron temperature, i.e. lower than the acceptable threshold for capsule preheat (< 0.5%) as shown in Fig. 2.

3.2 Hohlraum power scaling

A series of experiments using 2 ns flattop pulses and variable laser energy in the 5-13 kJ range was performed to measure the radiation temperature scaling with laser power and hohlraum size under conditions where minimal plasma filling is expected. Figure 3a shows measured and predicted radiation temperatures for scale-1 (1.6 mm diameter, 1.5 mm long) and scale-3/4 (1.2 mm diameter, 1.1 mm long) hohlraums with a LEH size of 0.75 of the hohlraum diameter, and the Dante view of the target and initial laser spots. We find that the radiation temperature scales as expected with both the laser power and hohlraum size from detailed LASNEX simulations [22] and from analytical scaling laws [25]. Moreover, the peak radiation temperature between Dante data and LASNEX calculations agree within the experimental Dante radiation temperature error bar of 2 %. Peak radiation temperatures similar to those required for the ICF design were measured. Furthermore, the measured soft x ray spectra of the hohlraum radiation were compared with simulations. Figure 4 shows radiation spectra recorded on the peak of the x ray drive for two different hohlraum radiation temperatures and post-processed from LASNEX simulations, showing good agreement over a wide temperature range. The highly efficient laser coupling to the hohlraums, i.e. the low levels of laser backscattering and hot electron fractions, contributed to the good agreement between the measured hohlraum x ray fluxes and the LASNEX predictions. Figures 3b and c show hard x ray side view images of the hohlraum emission at the end of the 2 ns pulse for a scale-1 and scale-3/4 hohlraum experiments conducted at the same laser power of 6.7 TW. In the scale-1 hohlraums the emission is localized at the back wall, confirming expectations of no plasma filling. The smaller scale-3/4 hohlraum also shows bright emission from the

back wall and some volume emission indicating that laser absorption by inverse bremsstrahlung in the LEH region becomes important at the end of the laser drive.

3.3 Plasma filling in long pulse hohlraums

Scale 1 and 3/2 hohlraums were heated by 6 and 9 ns long pulses to test hohlraum radiation production limits due to plasma filling. Measurements performed with Dante and thin wall imaging were compared with LASNEX simulations.

3.3.1 LASNEX simulations and thin wall imaging data

Figure 5 shows that when irradiated by a longer 6 ns laser pulse the Au L-shell emission in the LEH region for a scale-1 hohlraum (0.8 mm LEH) eventually dominates as a result of plasma filling. We apply LASNEX simulations to calculate the ablation from the gold hohlraum walls by soft x rays and the cylindrically inward motion of the ablated plasma. First, the laser deposits its energy at the back wall. The primary x rays emitted by the laser plasma at the back wall will heat and ablate the cylindrical wall. The x ray ablation plasma that is colder than the laser wall plasma moves radially into the beam path and is directly heated by the laser beams. This creates a high plasma pressure on the hohlraum axis retarding complete closure of the hohlraum, which is an important part of the hydrodynamics (Fig. 7 at 1 ns). Second, roll-over of the internal radiation temperature occurs at $\sim$ 4 ns when the ablated plasma moving inward from the LEH begins to significantly absorb and refract the laser beam at the LEH. According to LASNEX calculations, at this time the electron density in the LEH plasma reaches peak values that exceed 0.2 nc for electron temperatures of about 5 keV. These electron densities are

higher than the previously postulated [8] roll-over limits for hohlraum heating due to plasma filling.

By the end of the laser pulse the LEH plasma completely absorbs the laser beams. As a consequence, the hard x ray radiation production migrates from the hohlraum back wall to the region of the LEH, where hydrodynamic and coronal radiative losses become dominant loss factors, resulting in the decrease of the internal radiation temperature [26]. This behavior is well reproduced by LASNEX post processed calculations of the Au L-shell emission (Fig. 5b) particularly the sudden transition from back wall to LEH dominated emission at ~ 4ns.

3.3.2 Measured and predicted hohlraum filling as a function of laser drive and hohlraum size

In addition to the scale-1 hohlraum irradiated with a 6 ns laser pulse, we performed long pulse experiments using larger, scale-3/2 hohlraums (2.4 mm diameter, 2.25 mm long, 1.4 mm LEH) demonstrating that our LASNEX modeling correctly predicts the size scaling of plasma fill limits and the roll-over of the internal radiation temperature. With the same 6 ns laser pulse into the larger scale-3/2 hohlraum, the Au L-shell emission remains considerably stronger at the back wall than at the LEH, indicating that the hohlraum fill plasma density is moderate and that the laser still propagates into the hohlraum until the end of the laser pulse. However, when irradiating the same scale-3/2 hohlraum with a longer, 9 ns laser pulse of similar energy, we observe strong emission in the LEH starting at t = 7 ns.

Figure 6 shows the radiation temperature through the LEH T_{LEH} for the long pulse experiments measured by Dante, and simulated by LASNEX and corresponding hard x ray images. Figure 6 also shows the corresponding measured and simulated "M-band flux" (radiation > 2keV photon energies). Both the 9 ns scale-3/2 and the 6 ns scale-1 results (b and c) show two characteristic signatures of roll-over not seen in the 6 ns scale-3/2 result (a). Most prominent is the rise in Au M-band flux produced by the dense LEH plasma that absorbs the laser beams and that is located where its emission is fully visible by Dante. In order to infer a roll-over time τ from our experiments, we use the time of the sudden rise in Au M-band flux. Less prominent and simultaneous with the M-band flux rise is a sudden rise in T_{LEH} that occurs when the LEH plasma becomes dense enough to entirely stop the laser beams.

Further, Fig. 6 shows the calculated "internal T_R ", which is the radiation temperature that would drive an HED package or a capsule located inside the hohlraum. This calculation shows the "roll-over" of the internal T_R before the end of the laser pulse, at the time τ (Fig. 6b and c) when the LEH plasma is dense enough to absorb entirely the laser energy. As expected, this roll-over is coincident with the sudden rise in M-band emission, the rise in LEH temperature and the migration of the L-shell emission from the back wall to the LEH.

3.3.3 Hohlraum filling features in optical backscattering measurements

Although the laser backscattering values in these experiments were low, the time resolved optical spectra showed features that contributed to the physical picture deduced from LASNEX simulations, Dante measurements and hard x ray imaging. Figure 7

shows time resolved SBS spectra for scale 3/2 and 6 ns laser pulse with low plasma filling (Fig. 6a) and for the same hohlraum size driven by a 9 ns laser pulse that fills before the end of the laser pulse (Fig. 6b). At the beginning of the laser pulse both SBS spectra show a specular reflection feature at the wavelength of the laser pulse (351 nm). In addition the SBS spectrum for the 9 ns hohlraum that fills with plasma shows a red shifted SBS feature right after the roll-over time. The wavelength shift of 0.3 nm is consistent with a shift caused by an electron temperature in the LEH plasma of ~ 4 keV given by the LASNEX simulations.

Figure 8 shows the time resolved SRS spectrum measured for the smaller scale 1 hohlraum, the corresponding hard x ray images (see Figs. 5 and 6c) and simulated two-dimensional electron density and temperature maps of the hohlraum. The SRS spectrum is emitted at the fill time allowing us to estimate the lower limit for the electron density in the LEH plasma. An electron density range in the LEH plasma of up to 0.15 nc at 3.5 ns is estimated from the SRS assuming an electron temperature of ~ 4.5 keV given by LASNEX simulations. This is consistent with the peak electron density values at the LEH simulated by LASNEX that range from 0.12 n_c at 3 ns to 0.22 n_c at 4 ns. The SRS decreases considerably after 4.3 ns, before the end of the laser pulse, due to the fact that the electron density in the LEH plasma exceeds 0.25 n_c as confirmed also by the simulations (Fig. 8). After 4.3 ns the weak SRS emission shows a continuous red shifting, consistent with the further increase in the electron density. SRS gain calculations using LASNEX simulated plasma parameters confirmed a low SRS gain and the spectral range of the measured SRS spectrum.

3.3.4 Analytic model of plasma filling

In addition to detailed numerical simulations, these results can be understood and extrapolated to higher laser energies and powers by applying a simple analytic model for radiation temperature limits [26]. This model is based on the increased hydrodynamic losses and thin coronal radiative losses proportional to n_e^2 (n_e-electron density) [3] that occur when the laser absorption region migrates to the LEH as the hohlraum fills with plasma, leading to the roll-over in the internal radiation temperature. In our model these losses become important at the LEH when the inverse bremsstrahlung absorption length in the laser heated LEH plasma becomes shorter than the LEH radius. The plasma conditions for inverse bremsstrahlung are calculated by balancing x ray ablated plasma pressure with laser heated plasma pressure and balancing heat conduction losses with inverse bremsstrahlung heating [27].

The model also balances laser power converted to x rays with wall Marshak wave heating losses, omitting thermal radiation losses out of the LEH which are less important for the LEH sizes used here. A constant x ray conversion efficiency (C.E.) of 75% of the 100% absorbed laser energy is assumed, the later justified by the very low values of measured laser backscattering. The model gives the roll-over radiation temperature $T_{max}=T_R(\tau)$ in terms of laser power or energy, roll-over time τ and LEH radius r:

$$T_{max} = 1.0P_L^{0.2}/r^{0.2}\tau^{0.07} = 1.0E_L^{0.2}/r^{0.2}\tau^{0.27} \qquad (2)$$

where T_{max} is in heV units, the flattop laser power (energy) P_L (E_L) is in TW (kJ), the roll-over time τ is in ns and the LEH radius r is in cm. The middle expression in Eq. (2) is applicable when the laser is power limited and the (right-hand) expression is applicable when the pulse length is long enough that the laser is energy limited. In Eq. (2) the laser

energy E_L is the integrated laser power up to the roll-over time τ. The model also defines the optimum average hohlraum radius R as follows:

$$R = 0.09 P_L^{0.17} t^{0.31} r^{0.33} \quad (3)$$

In equation (3) the roll-over time is replaced with the laser pulse length t and it shows that the optimum hohlraum size increases only slowly with longer fill (roll-over) times τ and laser power or energy. The model can also be used to estimate the plasma conditions in the LEH plasma when the internal temperature rolls over:

$$n_e = 0.0145\ P_L^{0.2}/r^{0.7} \quad (4)$$

$$T_e = 1.34\ P_L^{0.3}/r^{0.3} \quad (5)$$

$$Zn_i = 0.18\ P_L^{0.3} t^{0.07}/r^{0.8} \quad (6)$$

where n_e and Zn_i are the electron and ion densities in units of critical density n_c, and T_e is the electron temperature in keV.

As shown in Fig. 6, the values of the simulated Dante T_{LEH} and internal T_R temperatures at the roll-over time are similar, which allows us to compare T_{max} (Eq. (2)) directly to the measured Dante temperature (T_{LEH}) at the roll-over time. Figure 9 plots the experimental Dante temperatures (full circles) at the roll-over times τ and the corresponding T_{max} limits calculated with Eq. (2) (crosses) showing good agreement. Included are data points for the scale 3/4 which showed significant LEH emission at the end of the pulse (Fig. 3a and c) and for a smaller scale-3/8 hohlraum, heated by a 1.1 ns laser pulse [24].

Figure 9 also shows analytical curves that describe the T_{max} limits (Eq. (2)) imposed by plasma filling for future experiments when the full NIF laser facility is used to heat hohlraums with 192 beams through two LEHs. The curve is calculated using Eq. (2) assuming a minimum LEH radius of 0.3 mm, dictated by the minimum NIF laser spot

size and a maximum angle of incidence of 50°. Extrapolating our analytic model predictions to full NIF hohlraum performance limits suggests a maximum achievable radiation temperature of T_{max} >700 eV.

We use Eqs. (2)-(6) to estimate the plasma conditions in these filled NIF hohlraums heated by the four beams, as well as using the full NIF laser (Fig. 9), an LEH radius of 0.3 mm and 1 ns at full power and 10 ns at full energy. Table 1 shows the calculated plasma parameters, optimal hohlraum size R (l=2R) and T_{max} (Eq. (2)) for the performed experiments that showed plasma filling and for the full NIF (Fig. 9). For the first NIF hohlraums with plasma filling we use the laser power and the roll-over time instead of the full laser energy. Considering the model's simplifying conditions, we find that for the scale 1 hohlraum at 6 ns (2.6 TW) the electron density (0.17 nc) and temperature (4.7 keV) estimates agree well with the LASNEX simulations (0.2 nc and 5 keV) (Figure 7). For full NIF this simple analytic model yields higher electron densities and temperatures at the filling limit, at considerably higher maximum radiation temperatures (Fig. 9). This shows that the full NIF system can provide a considerably hotter and/or longer hohlraum drive for HED applications than is required for ICF [1,2].

4. Summary

The first vacuum hohlraum experiments were used to activate NIF's hohlraum drive capability and to verify hohlraum drive scaling with laser power and hohlraum size. LASNEX was used to assess the radiation-driven hydrodynamics in the hohlraums. As shown in Figure 10, peak T_R Dante measurements agreed well with LASNEX simulations including for a higher-temperature scale 3/8 hohlraum [28] exceeding 300

eV, which is the ICF peak temperature. Simulations of hohlraum plasma filling were corroborated in long pulse experiments by finding good agreement between measurements and LASNEX simulations of hard x ray imaging and Dante soft x ray drive.. In addition, a simple analytic model used to estimate the radiation production limits fits the four beam NIF hohlraum performance limits for the highly filled hohlraums, and was further used to estimate hohlraum plasma conditions and upper limits on hohlraum performance for full NIF with 192 beams.

Acknowledgments

This work would not have been possible without a large team which includes the NIF operations staff, the Bechtel Nevada LO calibrations staff, the target area staff and valuable contributions from E.I. Moses, C.A. Haynam, F.A.Weber, R.L. Kauffman, B.K. Young, M.J. Shaw, R.E. Turner, D. Froula, D.G. Pellinen, B.R. Thomas*, L.J. Atherton, R.E. Bonanno, S.N. Dixit, D.C. Eder, G. Holtmeier, D.H. Kalantar, A.E. Koniges, B.J. MacGowan, K.R. Manes, D.H. Munro, J.R. Murray, T.G. Parham, K. Piston, B.M. Van Wonterghem, R.J. Wallace, P.J. Wegner, P.K. Whitman, , G. Armstrong, D.E. Bower, S.C. Burkhart, R. Costa, C. Gates, J. Grinold, D. Hargrove, M. Hermann, S. Johnson, J. Kamperschroer, J. Kimbrough, T. Kohut, M. Landon, C. Marshall, J. Menapace, V. Rekow, M. Rhodes, V. Roberts, A. Warrick, P. Watts, and P.E. Young. The authors would also like to thank M-C Monteil, CEA, France, and R.M. Stevenson, AWE, for valuable discussions. This work was performed under the auspices of the U.S. Department of Energy by the University of California, Lawrence Livermore National Laboratory under Contract No. W-7405-ENG-48.

References

[1] J.D. Lindl, Phys. Plasmas **2**, 3933 (1995).

[2] J.D. Lindl et al., Phys. Plasmas **11**, 339 (2004).

[3] L.J. Suter et al., Phys. Plasmas **3,** 2057 (1996).

[4] J. Massen et al., Phys. Rev. E **50**, 5130 (1994).

[5] A. Benuzzi et al., Phys. Rev E **54**, 2162 (1996).

[6] B. Remington et al., Metallurgical and Mat. Trans. A, **35A**, 2587 (2004).

[7] C.A. Back et al., Phys. Rev. Lett. **84**, 274 (2000).

[8] B. Thomas, AWE, private communication, 1995.

[9] S.H. Glenzer et al., Phys. Rev. Lett. **80**, 2845 (1998).

[10] E. Dattolo et al., Phys. Plasmas **8**, 260 (2001).

[11] G.D. Tsakiris and R. Sigel, Phys. Rev. A **38**, 5769 (1988).

[12] R.M. Stevenson et al., Phys. Rev. Lett. **94**, 055006 (2005).

[13] G.H. Miller, E.I. Moses and C.R. Wuest, Nucl. Fusion **44,** 228 (2004).

[14] S.H. Glenzer et al., Nucl. Fusion **44**, 185 (2004).

[15] J.A. Menapace, S.N. Dixit, F.Y. Genin, W.F. Brocious, Proc. SPIE **5273**, 220 (2003).

[16] D. H. Munro, S. N. Dixit, A. B. Langdon, J. R. Murray, Appl. Opt. **43**, 6639 (2004).

[17] L.J. Suter et al., Rev. Sci. Instrum. **68**, 838 (1997).

[18] E.L. Dewald et al., Rev. Sci. Instrum. **75**, 3759 (2004).

[19] J.W. McDonald et al., Rev. Sci. Instrum. **75**, 3753 (2004).

[20] D. Froula et al., Rev. Sci. Instrum. **75**, 4168 (2004).

[21] A.J. Mackinnon et al., Rev. Sci. Instrum. **75**, 4183 (2004).

[22] G.B. Zimmerman and W.L. Kruer, Comm. Plasma Phys. Contr. Fusion **2**, 51 (1975).

[23] L.J. Suter et al., Phys. Rev. Lett **73**, 2328 (1994).

[24] J.W. McDonald et al., submitted to Phys. Plasmas, 2005.

[25] R. Sigel et al., Phys. Rev. Lett. **65**, 587 (1990).

[26] E.L. Dewald, L.J. Suter, O.L. Landen et al., Phys. Rev. Letters 2005, to be published.

[27] T.W. Johnston and J.M. Dawson, Phys. Fluids **16**, 722 (1973).

[28] D. Hinkel et al., Phys. Plasmas, **12**, 056305 (2005).

Figure captions

Figure 1. Experimental layout and design of diagnostics and target chamber; typical measured data are also shown.

Figure 2. Measured hot electron fraction as a function of laser intensity for the NIF hohlraum experiments (squares), and from previous NOVA hohlraum data (triangles); also represented is the f_{hot} threshold for ignition designs. Hohlraums that fill with plasma (solid points) show increased f_{hot} .

Figure 3. Dante view and radiation temperature measurements of hohlraum targets with initial laser spots on the wall shown as dark circle. (a) Radiation temperature measured with Dante (continuous lines) and calculated (dashed lines) for 2 ns flattop laser pulses and variable hohlraum scale and laser power; Gated x ray (> 9 keV) side view images at 1.9 ns for 6.7 TW drive in (b) scale-1 and (c) 3/4 hohlraums.

Figure 4. Spectra on the peak of the x ray drive measured with Dante and simulated by LASNEX for two different hohlraum radiation temperatures.

Figure 5. (a) Measured and (b) calculated hard x ray (> 9 keV) gated images in Scale-1 hohlraum heated by 2.7 TW, 6 ns laser pulse. (c) Cross-section of electron density profiles and laser ray propagation calculated with 2D Lasnex code.

Figure 6. Radiation temperature history as measured by Dante through LEH (continuous thick line) and as simulated by LASNEX (full squares). Circles are predicted internal radiation temperatures. Measured (continuous thin line) and calculated (triangles) M-band (>2 keV) flux are plotted on RHS scale. Measured and hard x ray (> 9 keV) gated images at different times. (a) scale-3/2 hohlraum driven by 2.7 TW in 6 ns, (b) scale-3/2 driven by 1.9 TW in 9 ns and (c) scale-1 driven by 2.7 TW in 6 ns flattop laser pulse.

Figure 7 Measured streaked SBS spectra for scale 3/2 hohlraums driven by (a) 2.7 TW in 6 ns, (b) and by 1.9 TW in 9 ns (Fig. 6a and b).

Figure 8 Measured streaked SRS spectrum for scale-1 hohlraum driven by 2.7 TW in 6 ns flattop laser pulse (Fig. 5 and 6a), the corresponding hard x ray images and 2-dimensional electron density temperature maps simulated with LASNEX.

Figure 9 Dante measured temperatures T_{LEH} at the roll-over time τ and the corresponding analytical limits (crosses) calculated with Eq. (2) using experimental values of LEH radius r and laser power. Continuous line is Eq. (6) analytic model limits for a constant LEH radius r = 0.3 mm for 600 TW, 1.8 MJ NIF hohlraum.

Figure 10. Measured and calculated peak radiation temperatures during the first NIF hohlraum experiments.

Table 1

Facility	**P_L**	**E_L**	**t**	**R**	**n_e**	**T_e**	**Zn_i**
units	TW	kJ	ns	mm	$/n_c$	keV	$/n_c$
NIF 1q	9		1	0.41	0.26	7.3	6
NIF 1q		13.5	2	0.54	0.19	6	4
NIF 1q	2.6		4	0.6	0.17	4.7	3.45
NIF 1q	1.9		7.5	0.74	0.12	3.7	2.4
NIF	600		1	0.84	0.61	26	20
NIF		1800	10	1.4	0.42	18	16

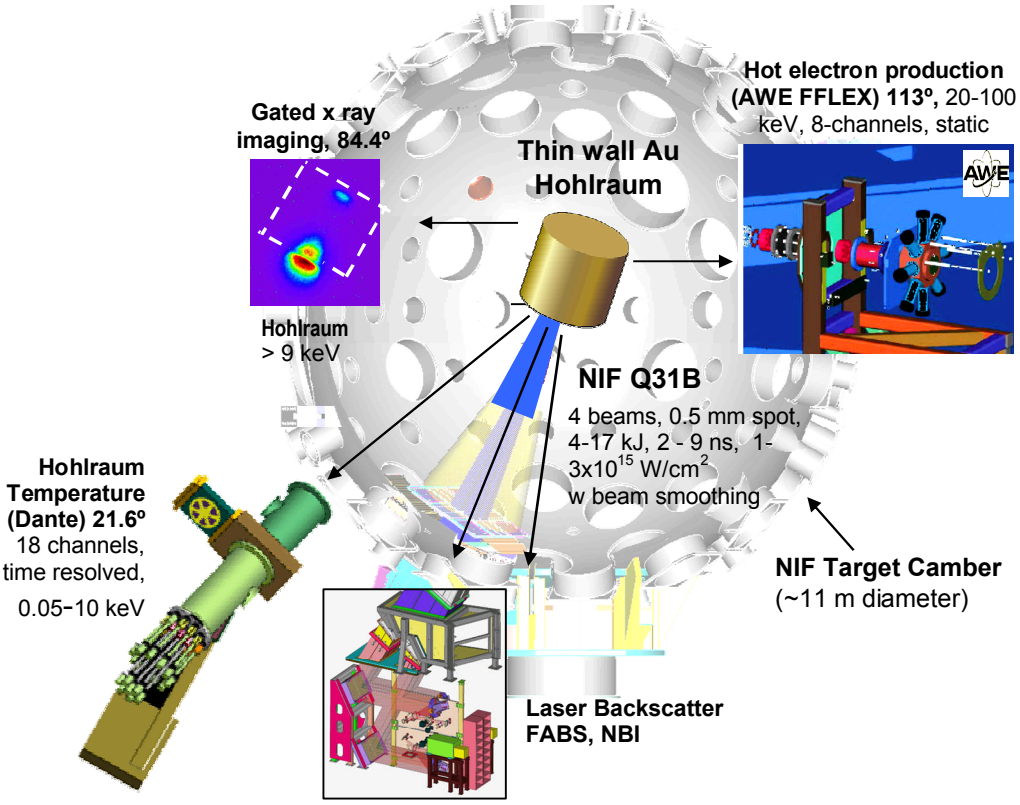
Gated x ray imaging, 84.4º
Thin wall Au Hohlraum
Hot electron production (AWE FFLEX) 113º, 20-100 keV, 8-channels, static
Hohlraum > 9 keV
NIF Q31B
4 beams, 0.5 mm spot, 4-17 kJ, 2 - 9 ns, 1-3x10^15 W/cm^2 w beam smoothing
Hohlraum Temperature (Dante) 21.6º 18 channels, time resolved, 0.05-10 keV
NIF Target Camber (~11 m diameter)
Laser Backscatter FABS, NBI

Figure 1

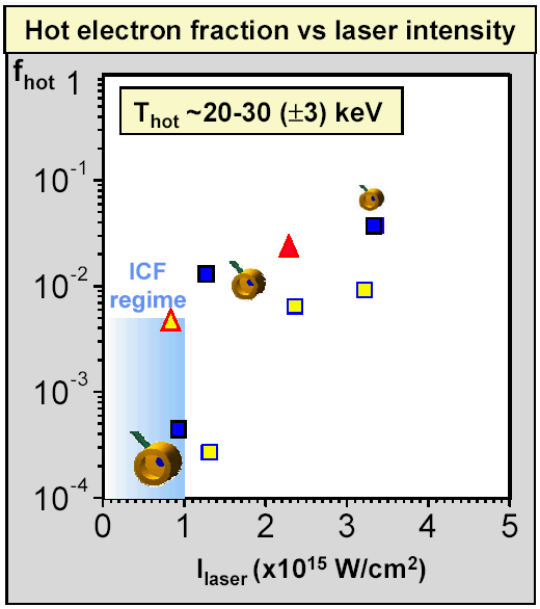
Hot electron fraction vs laser intensity
f_{hot}
1
10^{-1}
10^{-2}
10^{-3}
10^{-4}
T_{hot} ~20-30 (±3) keV
ICF
regime
0
1
2
3
4
5
I_{laser} (x10^{15} W/cm^2)

Figure 2

Figure 3

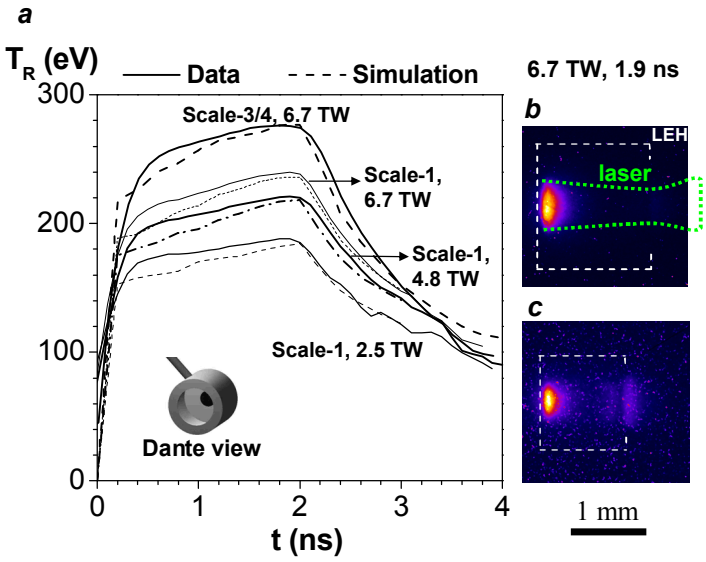
a
T_R (eV)
Data
Simulation
300
200
100
0
0
1
2
3
4
t (ns)
Scale-3/4, 6.7 TW
Scale-1, 6.7 TW
Scale-1, 4.8 TW
Scale-1, 2.5 TW
Dante view
6.7 TW, 1.9 ns
b
LEH
laser
c
1 mm

Fig.4

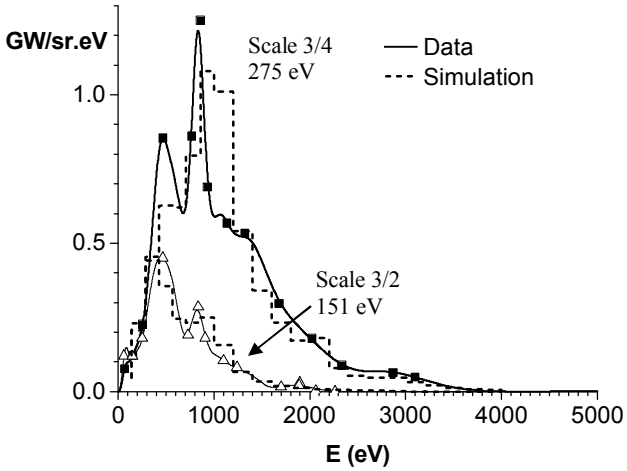
GW/sr.eV
1.0
0.5
0.0
0
1000
2000
3000
4000
5000
E (eV)
Scale 3/4
275 eV
Scale 3/2
151 eV
Data
Simulation

Figure 5

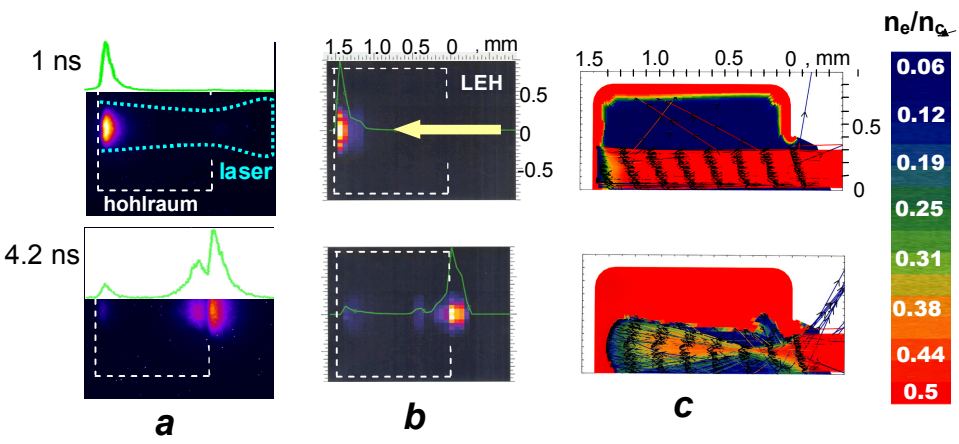

Formatted

Figure 6

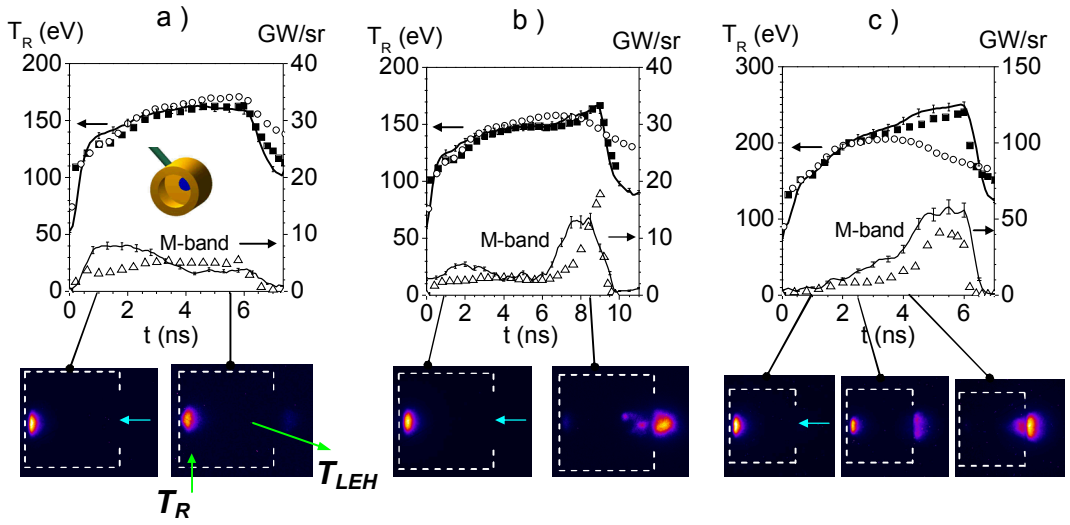

Figure 7

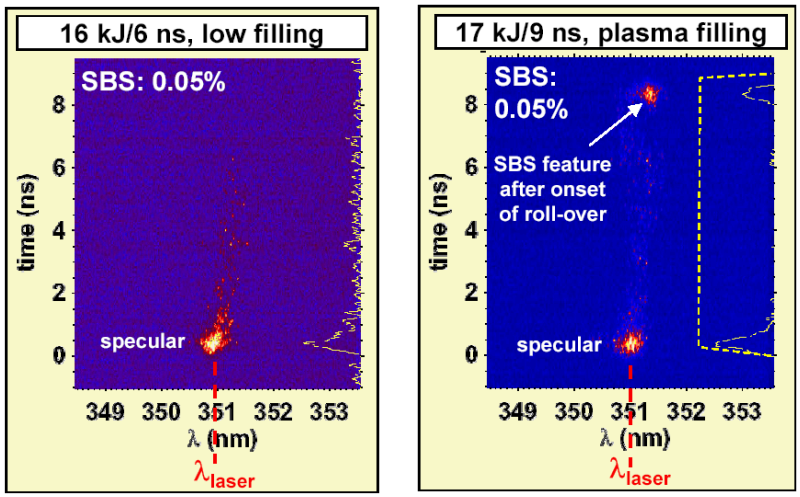
16 kJ/6 ns, low filling
SBS: 0.05%
time (ns)
8
6
4
2
0
specular
349 350 351 352 353
λ (nm)
λlaser
17 kJ/9 ns, plasma filling
SBS:
0.05%
SBS feature
after onset
of roll-over
time (ns)
8
6
4
2
0
specular
349 350 351 352 353
λ (nm)
λlaser

Figure 8

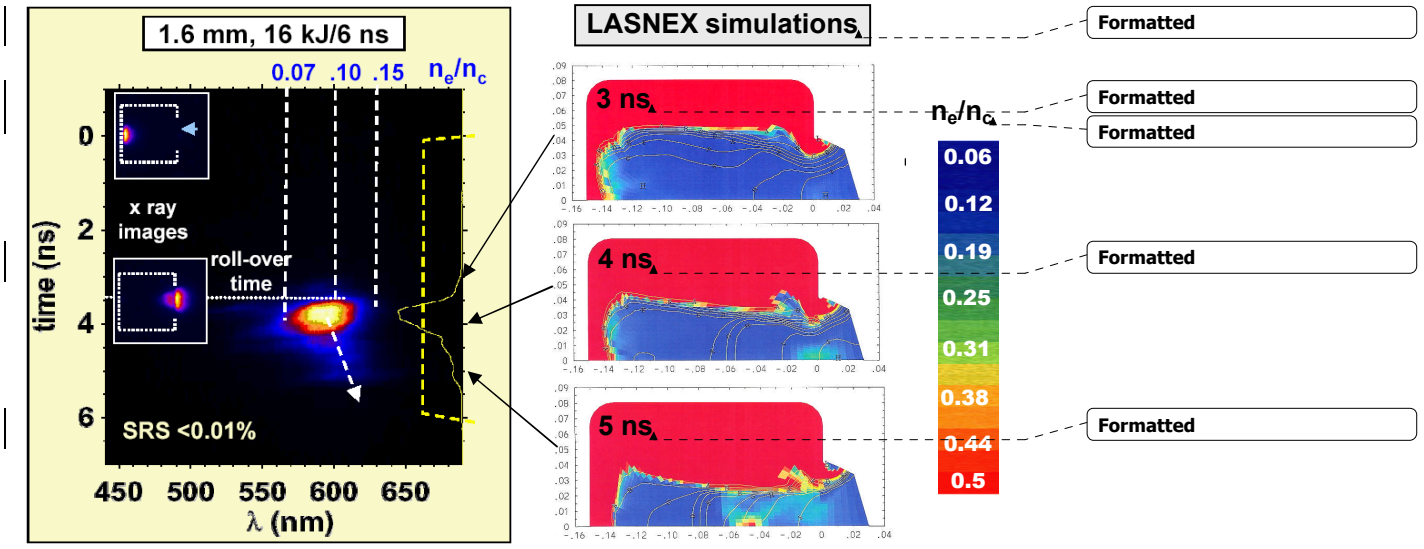
1.6 mm, 16 kJ/6 ns
0.07 .10 .15 n_e/n_c
x ray images
roll-over time
SRS <0.01%
time (ns)
0
2
4
6
450 500 550 600 650
λ (nm)
LASNEX simulations
3 ns
4 ns
5 ns
n_e/n_c
0.06
0.12
0.19
0.25
0.31
0.38
0.44
0.5
Formatted
Formatted
Formatted
Formatted
Formatted

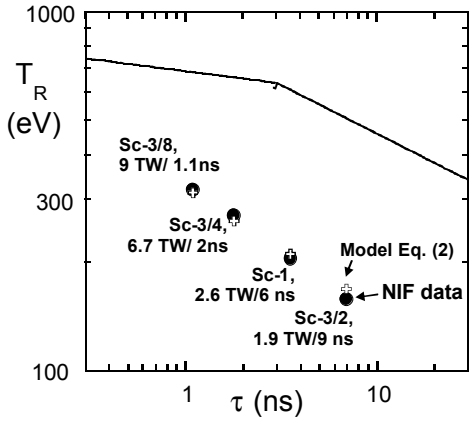
1000
T
R
(eV)
300
100
Sc-3/8,
9 TW/ 1.1ns
Sc-3/4,
6.7 TW/ 2ns
Sc-1,
2.6 TW/6 ns
Sc-3/2,
1.9 TW/9 ns
Model Eq. (2)
NIF data
1
τ (ns)
10

Figure 9

Figure 10

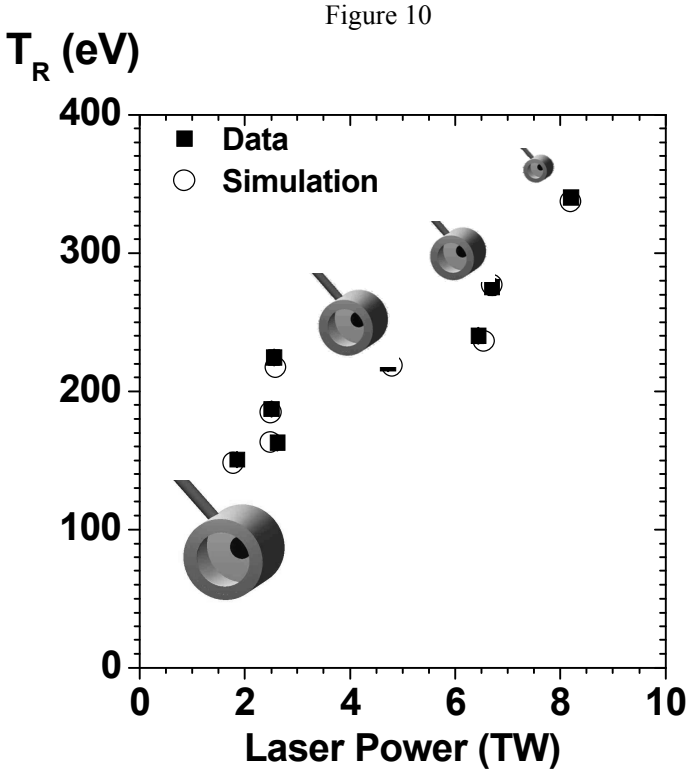
T_R (eV)
400
300
200
100
0
Data
Simulation
0
2
4
6
8
10
Laser Power (TW)